

Deep neural network solution of the electronic Schrödinger equation

Jan Hermann^{1,2,*}, Zeno Schätzle¹, and Frank Noé^{1,3,4,*}

¹*FU Berlin, Department of Mathematics and Computer Science, Arnimallee 6, 14195 Berlin, Germany*

²*TU Berlin, Machine Learning Group, Marchstr. 23, 10587 Berlin, Germany*

³*FU Berlin, Department of Physics, Arnimallee 14, 14195 Berlin, Germany*

⁴*Rice University, Department of Chemistry, Houston, TX 77005, USA*

Abstract The electronic Schrödinger equation describes fundamental properties of molecules and materials, but cannot be solved exactly for larger systems than the hydrogen atom. Quantum Monte Carlo is a suitable method when high-quality approximations are sought, and its accuracy is in principle limited only by the flexibility of the used wave-function ansatz. Here we develop a deep-learning wave-function ansatz, dubbed PauliNet, which has the Hartree–Fock solution built in as a baseline, incorporates the physics of valid wave functions, and is trained using variational quantum Monte Carlo (VMC). Our deep-learning method achieves higher accuracy than comparable state-of-the-art VMC ansatzes for atoms, diatomic molecules and a strongly-correlated hydrogen chain. We anticipate that this method can reveal new physical insights and provide guidance for the design of molecules and materials where highly accurate quantum-mechanical solutions are needed, such as in transition metals and other strongly correlated systems.

1 Introduction

A cornerstone of predicting the physical and chemical properties of a given molecule or material is the solution of the corresponding time-independent electronic Schrödinger equation, which describes the distribution and energy of its electrons (Szabo and Ostlund, 1996). In this equation, the investigated molecule is specified by the Hamiltonian differential operator, \hat{H} , and the unknowns are the electronic wave function, $\psi(\mathbf{r}_1, \dots, \mathbf{r}_N)$, and electronic energy, E ,

$$\hat{H}\psi(\mathbf{r}_1, \dots, \mathbf{r}_N) = E\psi(\mathbf{r}_1, \dots, \mathbf{r}_N) \quad (1)$$

$$\hat{H} := \sum_i \left(-\frac{1}{2} \nabla_{\mathbf{r}_i}^2 - \sum_I \frac{Z_I}{|\mathbf{r}_i - \mathbf{R}_I|} \right) + \sum_{i < j} \frac{1}{|\mathbf{r}_i - \mathbf{r}_j|} \quad (2)$$

Here, $(\mathbf{r}_1, \dots, \mathbf{r}_N) \equiv \mathbf{r} \in \mathbb{R}^{3N}$ are the spatial coordinates of N electrons, and (Z_I, \mathbf{R}_I) are the charges and coordinates of M atomic nuclei, considered to be fixed under the Born–Oppenheimer approximation. Electrons have in principle also spin coordinates, $s_i \in \{\uparrow, \downarrow\}$, but these can be considered fixed, because the Hamiltonian \hat{H} does not operate on spins. As electrons are fermions, the electronic wave function must be antisymmetric with respect to the exchange of the spatial coordinates of any two electrons with equal spin ($s_i = s_j$),

$$\psi(\dots, \mathbf{r}_i, \dots, \mathbf{r}_j, \dots) = -\psi(\dots, \mathbf{r}_j, \dots, \mathbf{r}_i, \dots), \quad (3)$$

The electronic Schrödinger equation can be solved analytically only for $N = M = 1$, the hydrogen atom. However, over the last 90 years the field of quantum chemistry has been remarkably successful in developing numerical methods to solve the Schrödinger equation approximately (Piela, 2014). These methods have varying degrees of accuracy and computational efficiency, with the

fundamental constraint that due to the antisymmetry of the electronic wave function, the computational problem is NP-hard (exponentially) with respect to N for a fixed level of accuracy (Troyer and Wiese, 2005). The goal of any approximate method is then to bring the computational cost to the polynomial regime (of varying degree), while sacrificing as little accuracy as possible.

Many methods of quantum chemistry build on the *variational principle*, which states that the solution of the Schrödinger equation with the lowest energy (the ground state), ψ_0 , E_0 , can be obtained by minimizing the energy expectation value over all possible antisymmetric wave functions. Thus, minimizing over a *trial* subset of all wave function, called an *ansatz*, parametrized by θ , gives an upper bound to the true ground-state energy E_0 :

$$E_0 = \min_{\psi} E[\psi] \leq \min_{\theta} E[\psi_{\theta}] \quad (4)$$

$$E[\psi] = \int d\mathbf{r} \psi(\mathbf{r}) \hat{H} \psi(\mathbf{r}) \quad (5)$$

In traditional approaches, such as the Hartree–Fock (HF) method or the coupled cluster method (Van Voorhis and Head-Gordon, 2000), the ansatzes are formed from linear combinations of a finite number of basis functions, with the linear coefficients being θ , such that the integral in (5) can be evaluated analytically, which turns the minimization problem in (4) into an algebraic equation for θ . An alternative path of using arbitrarily complicated ansatzes and evaluating the energy integral numerically is taken by the variational quantum Monte Carlo (VMC) (Foulkes et al., 2001; Needs et al., 2010; Austin et al., 2012). In this approach, the energy integral is written as an expected value of the *local energy*, $E_{\text{loc}}[\psi](\mathbf{r}) = \hat{H}\psi(\mathbf{r})/\psi(\mathbf{r})$, over the probability distribution $|\psi^2(\mathbf{r})|$,

$$E[\psi] = \mathbb{E}_{\mathbf{r} \sim |\psi|^2} [E_{\text{loc}}[\psi](\mathbf{r})] \quad (6)$$

Practical VMC calculations are usually followed by diffusion quantum Monte Carlo (DMC), which can further lower the upper bound to the true ground-state energy. DMC is in principle exact, but attempting to use it to improve the *nodal surface* of a

*Emails: jan.hermann@fu-berlin.de, frank.noe@fu-berlin.de

wave-function ansatz leads to an exponentially growing numerical noise, which is just a manifestation of the aforementioned NP-hardness. The nodal surface is the hyperplane of electronic coordinates on which the wave function changes sign, so the NP-hardness of the electronic problem is often referred to as the *sign problem* (Ceperley, 1991). As a result, DMC calculations are almost always performed with the nodal surface fixed by the preceding VMC calculation, which sets the fundamental limitation to the accuracy of quantum Monte Carlo (QMC) techniques. This is the first reason to try to improve existing wave-function ansatzes. The second reason is that it has been difficult to extend DMC to molecular properties beyond the electronic energy, whereas it is straightforward to calculate a number of properties from an optimized VMC wave function.

The existing wave-function ansatzes are partially motivated by the physics of electrons, partially by trial-and-error experience. In many other computational fields, deep neural networks (DNNs) as universal function approximators proved to outperform handcrafted solutions based on experience, leading naturally to the question whether VMC is prone to such a disruption as well. Here, we demonstrate that ansatzes that incorporate the right physics while using DNNs in place of the existing ad-hoc functional forms indeed can outperform state-of-the-art variational ansatzes of comparable types. In particular, we present a DNN architecture that represents electronic wave functions with the required antisymmetry and encodes further relevant physical knowledge such as nuclear and electronic cusp conditions. On a small set of test systems, we show that this architecture gives access to wave functions with energies comparable to those that could have been previously obtained only with DMC.

The idea to represent wave functions with neural networks in the context of VMC has been first presented and explored by Carleo and Troyer (2017) for discrete spin lattice systems. The first application of VMC with DNN wave functions for molecules, dubbed DeepWF, was reported by Han et al. (2018). However, their ansatz fails to reach the accuracy of even the baseline HF method for some systems. While we were preparing this manuscript, a preprint by Pfau et al. (2019) appeared, reporting a successful implementation of the same basic idea which differs in several technical details from ours. Most importantly, their DNN architecture does not have as much physical knowledge directly built in, which is compensated by a much larger number of parameters in θ , resulting in higher accuracy but also more computationally demanding optimization of their ansatz compared to our architecture.

2 PauliNet structure and optimization

2.1 Deep Slater–Jastrow–backflow ansatz incorporating the physics of electrons

Some parts of standard electronic wave-function forms are motivated by physics, other parts are simply a result of experimentation. In this section, we describe a deep-learning architecture that keeps the physically-motivated parts and replaces the ad-hoc parts with DNNs.

Our proposed wave function ansatz, dubbed PauliNet, is of the Slater–Jastrow–backflow type, where both the Jastrow factor J and the backflow \mathbf{f} are represented by DNNs with trainable pa-

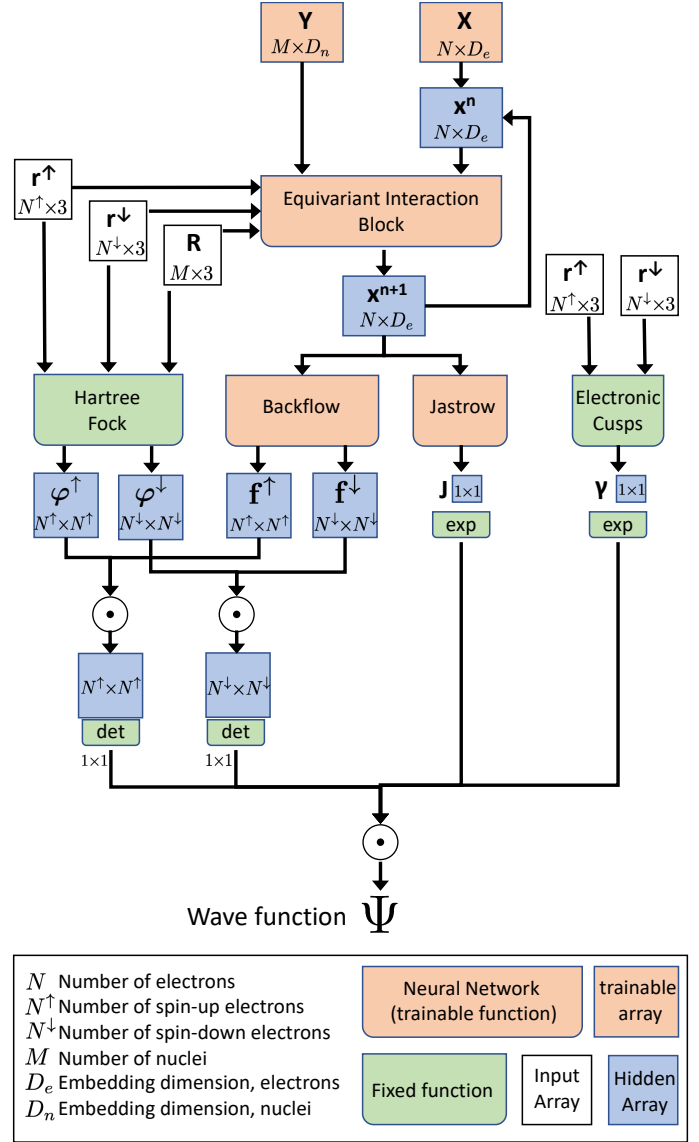


Figure 1 | Schematic of the PauliNet structure and information flow.

rameters θ (Figure 1),

$$\psi_{\theta}(\mathbf{r}) = \det[\varphi_{\mu}(\mathbf{r}_i^{\uparrow})f_{\theta,\mu i}(\mathbf{r})] \det[\varphi_{\mu}(\mathbf{r}_i^{\downarrow})f_{\theta,\mu i}(\mathbf{r})] e^{\gamma(\mathbf{r}) + J_{\theta}(\mathbf{r})} \quad (7)$$

The Jastrow factor and backflow DNNs are invariant and equivariant, respectively, with respect to the exchange of same-spin electrons, and φ_{μ} and γ are fixed functions. This functional form ensures the basic physics of electronic wave functions, as explained below.

Antisymmetry Since the electron spins are fixed due to the absence of any spin operator in the Hamiltonian, and to simplify notation, we assume the first N_{\uparrow} (N_{\downarrow}) electrons to be spin-up (spin-down),

$$\psi(\mathbf{r}_1^{\uparrow}, \dots, \mathbf{r}_{N_{\uparrow}}^{\uparrow}, \mathbf{r}_{N_{\uparrow}+1}^{\downarrow}, \dots, \mathbf{r}_N^{\downarrow}) \equiv \psi(\mathbf{r}^{\uparrow}, \mathbf{r}^{\downarrow}) \equiv \psi(\mathbf{r}) \quad (8)$$

The wave function then must be antisymmetric in the first N_{\uparrow} and in the last $N_{\downarrow} = N - N_{\uparrow}$ coordinates (eq. 3). An important consequence of the antisymmetry is that the wave function

goes through zero on the hyperplanes where same-spin electron coordinates coincide, resulting in zero probability density to observe such occurrences, which is called the Pauli exclusion principle, hence the name of our DNN ansatz. Antisymmetry must be enforced by the architecture, because the variational principle in (4) is only valid with this constraint. Without this constraint, the lowest-energy wave function would be always totally symmetric.

As is common in quantum chemistry, our ansatz in eq. 7 enforces antisymmetry among same-spin electrons via a matrix determinant, as the determinant of a matrix changes sign upon exchanging any two of its rows (or columns).

Hartree–Fock baseline To ensure a good starting point for the variational optimization problem, we take advantage of a well-established general wave-function form from quantum chemistry, and build the HF solution as a baseline into our model. The HF wave function uses a set of one-electron functions, $\varphi_\mu(\mathbf{r})$, called molecular orbitals, and their so-called Slater determinant to ensure antisymmetry,

$$\psi_{\text{HF}}(\mathbf{r}) := \det[\varphi_\mu(\mathbf{r}_i^\uparrow)] \det[\varphi_\mu(\mathbf{r}_i^\downarrow)] \quad (9)$$

The molecular orbitals are expressed as a linear combination of basis functions centered on the atomic nuclei, and the linear coefficients that minimize the energy can be easily found by solving an algebraic equation with a fixed-point iteration. In quantum chemistry, the HF method is usually considered a baseline method, as it is straightforward, computationally efficient, captures much of the basic physics of atoms and molecules, and makes qualitative reasonable predictions.

The single-electron molecular orbitals φ_μ are fixed in our ansatz and taken from the HF method, ensuring a good initial starting point for the variational optimization. Since the HF solution serves here only as a initial guess for the wave function, we can use a relatively small basis set.

Beyond Hartree–Fock with trainable Jastrow factor and backflow The HF method lacks any reference to interelectronic distances, and as a result does not capture any correlation between the electrons besides the antisymmetric constraint. Due to this limitation, the HF method has limited quantitative performance and even exhibits qualitative errors for so-called strongly-correlated systems. Our ansatz combines two established VMC strategies to improve over the HF baseline.

First, the HF wave function is multiplied by a nonnegative totally symmetric function $e^{J(\mathbf{r})}$, with J being the Jastrow factor (Drummond et al., 2004). This modification can build complex electron correlations into the wave function, but since it is always nonnegative, it cannot modify the nodal surface inherited from the HF wave function.

Second, one can generalize the molecular orbitals to be functions of all the electron coordinates as long as their equivariance (and thus the determinant antisymmetry) with respect to the exchange of same-spin electrons is retained,

$$\varphi_\mu(\mathbf{r}_i) \rightarrow \varphi_{\mu i}(\mathbf{r}), \quad \mathcal{P}\varphi_{\mu i}(\mathbf{r}) = \varphi_{\mu i}(\mathcal{P}\mathbf{r}) \quad (10)$$

where \mathcal{P} is the exchange operator for same-spin electrons. This approach is called the backflow, and unlike the Jastrow factor it

can modify the nodal surface of the HF wave function. In standard VMC, the backflow is achieved by keeping φ_μ intact, but generalizing the single-electron coordinates into collective quasi-coordinates (López Ríos et al., 2006). Recently, the backflow has been also used in combination with DNNs in discrete lattice models of electrons (Luo and Clark, 2019). In our ansatz, the backflow is achieved by multiplying the orbitals $\varphi_\mu(\mathbf{r}_i)$ with trainable backflow DNN functions $f_{\theta, \mu i}$.

We design the Jastrow factor and backflow DNNs to be invariant and equivariant, respectively, with respect to exchange of same-spin electrons (see Sec. 2.2),

$$\begin{aligned} J(\mathcal{P}\mathbf{r}) &= J(\mathbf{r}) \\ \mathcal{P}f_{\mu i}(\mathbf{r}) &= f_{\mu i}(\mathcal{P}\mathbf{r}) \end{aligned} \quad (11)$$

Cusp conditions In addition to the antisymmetry, any ground-state electronic wave function obeys exact asymptotic behavior defined by the *cusp conditions* as electrons approach each other and the nuclei (Kato, 1957). These conditions result from the potential terms in (2) diverging as the interparticle distance goes to zero, which must be compensated by a corresponding but opposite divergence of the Laplace operator in the kinetic term.

$$\left. \frac{1}{\psi_0} \frac{\partial \psi_0}{\partial |\mathbf{r}_i - \mathbf{R}_I|} \right|_{\mathbf{r}_i = \mathbf{R}_I} = -Z_I \quad (12)$$

$$\left. \frac{1}{\psi_0} \frac{\partial \psi_0}{\partial |\mathbf{r}_i - \mathbf{r}_j|} \right|_{\mathbf{r}_i = \mathbf{r}_j} = \begin{cases} \frac{1}{4} & s_i = s_j \\ \frac{1}{2} & s_i \neq s_j \end{cases} \quad (13)$$

While the cusp conditions could be learned from the variational principle, building them directly into the functional form of the wave-function has two advantages: (i) Starting with a better guess of the exact wave function achieves more efficient optimization. (ii) Without the cusp conditions, the local energy diverges and wildly oscillates around the coalescence points, which makes the optimization via the variational principle numerically unstable.

Eq. 7 ensures the nuclear cusp conditions in (12) via the molecular orbitals $\varphi_\mu(\mathbf{r}_i)$. We achieve this by modifying the molecular orbitals using the technique from Ma et al. (2005) with one simplification. In particular, we optimize the orbital values at atomic nuclei, $\mathbf{r}_i = \mathbf{R}_I$, via the energy variational principle, rather than fitting them against references values.

The electronic cusp conditions in (13) are enforced by $\gamma(\mathbf{r})$,

$$\gamma(\mathbf{r}) := \sum_{i < j} -\frac{c_{ij}}{1 + |\mathbf{r}_i - \mathbf{r}_j|}, \quad (14)$$

where c_{ij} is either $\frac{1}{2}$ or $\frac{1}{4}$ depending on the spins of the two electrons, according to (13).

To preserve the cusp conditions built into φ_μ and γ , the Jastrow factor and backflow DNNs must be cusplless,

$$\nabla_{\mathbf{r}_i} J(\mathbf{r}) \Big|_{\mathbf{r}_i = \{\mathbf{r}_k, \mathbf{R}_a\}} = 0, \quad \nabla_{\mathbf{r}_i} f_{\mu i}(\mathbf{r}) \Big|_{\mathbf{r}_i = \{\mathbf{r}_k, \mathbf{R}_a\}} = 0 \quad (15)$$

These conditions are ensured by construction of the DNNs, as detailed below.

2.2 Neural network architecture

Next, we discuss the architecture of the DNNs representing the Jastrow factor J and the backflow \mathbf{f} . The requirements of in-

variance and equivariance with respect to permutation of particles, and the fact that particle interactions are a function of their distances are closely related with the aim of constructing DNNs that learn potential energy functions. Therefore, we employ and adapt SchNet (Schütt et al., 2018), which is a DNN architecture that has been developed to represent quantum-chemical energy surfaces. SchNet is an instance of the class of graph convolutional neural networks, and was designed to model the electronic energy as a function of just the nuclear charges and coordinates, $E(\{(Z_I, \mathbf{R}_I)\})$. In a concise mathematical form, the SchNet architecture can be expressed as

$$\begin{aligned} \mathbf{x}_I^{(0)} &:= \mathbf{X}_{\theta, Z_I} \\ \mathbf{z}_I^{(n)} &:= \sum_{J \neq I} \mathbf{w}_{\theta}^{(n)}(\mathbf{e}(|\mathbf{R}_I - \mathbf{R}_J|)) \odot \mathbf{h}_{\theta}^{(n)}(\mathbf{x}_J^{(n)}) \\ \mathbf{x}_I^{(n+1)} &:= \mathbf{x}_I^{(n)} + \mathbf{g}_{\theta}^{(n)}(\mathbf{z}_I^{(n)}) \\ E &:= \sum_I \epsilon_{\theta}(\mathbf{x}_I^{(N)}) \end{aligned} \quad (16)$$

where “ \odot ” denotes element-wise multiplication, \mathbf{X}_{θ, Z_I} are trainable atom embeddings, $\mathbf{w}_{\theta}^{(n)}$, $\mathbf{h}_{\theta}^{(n)}$, $\mathbf{g}_{\theta}^{(n)}$, and ϵ_{θ} are trainable functions represented by ordinary fully-connected DNNs, and \mathbf{e} is a function that featurizes the interatomic distances. SchNet has been previously extended and used outside its original scope to represent finite-basis expansions of electronic wave functions (Schütt et al., 2019).

Our modifications of SchNet are as follows. (i) Since the wave function is a function of electron coordinates, the iterated feature vectors $\mathbf{x}_i^{(n)}$ represent electrons, not atoms, and we only distinguish two initial embeddings, for spin-up and spin-down electrons, because electrons are otherwise indistinguishable. (ii) The messages $\mathbf{z}_i(n)$ received by the electron feature vectors at each iteration are split into three channels, corresponding to same-spin electrons (+), opposite-spin electrons (−), and the nuclei (n). This builds more flexibility into the architecture, and is motivated by the fact electrons and nuclei are particles of entirely different type. (iii) Each channel has a separate receiving function \mathbf{g}_{θ} , again increasing flexibility without substantially increasing the number of parameters. (iv) Each nucleus is represented by a trainable embedding $\mathbf{Y}_{\theta, I}$, which is shared across all iterations and not iteratively updated. In VMC, the wave function is always optimized for a given fixed geometry of the nuclei, so the nuclear embeddings can be assumed to already represent each nucleus with its (fixed) atomic environment, hence the absence of need for their iterative refinement. (v) Two new trainable functions η_{θ} and κ_{θ} return the values of the Jastrow factor and the backflow, respectively, calculated from the electron feature vectors after the final iteration. These are the equivalent of the atomic-energy function ϵ_{θ} from the original SchNet. Since the feature vectors $\mathbf{x}_i^{(n)}$ are equivariant with respect to exchange at each iteration, so are the backflow vectors \mathbf{f}_i . (vi) The distance features \mathbf{e} are constructed to be cusplless, as detailed below. In short, the adapted SchNet

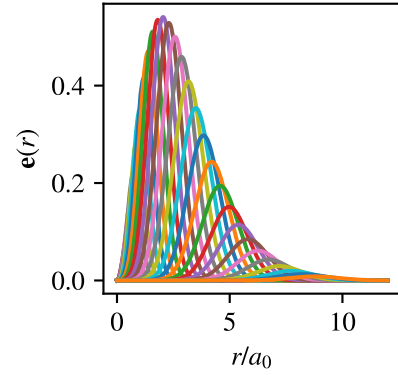


Figure 2 | Plot of the Gaussian distance featurization $\mathbf{e}(r)$. The plot is shown for the choice of 32 features and the cutoff $r_c = 10a_0$.

architecture is written as

$$\begin{aligned} \mathbf{x}_i^{(0)} &:= \mathbf{X}_{\theta, s_i} \\ \mathbf{z}_i^{(n, \pm)} &:= \sum_{j \neq i}^{\pm} \mathbf{w}_{\theta}^{(n, \pm)}(\mathbf{e}(|\mathbf{r}_i - \mathbf{r}_j|)) \odot \mathbf{h}_{\theta}^{(n)}(\mathbf{x}_j^{(n)}) \\ \mathbf{z}_i^{(n, n)} &:= \sum_I \mathbf{w}_{\theta}^{(n, n)}(\mathbf{e}(|\mathbf{r}_i - \mathbf{R}_I|)) \odot \mathbf{Y}_{\theta, I} \\ \mathbf{x}_i^{(n+1)} &:= \mathbf{x}_i^{(n)} + \sum_{\pm} \mathbf{g}_{\theta}^{(n, \pm)}(\mathbf{z}_i^{(n, \pm)}) + \mathbf{g}_{\theta}^{(n, n)}(\mathbf{z}_i^{(n, n)}) \\ J &:= \eta_{\theta}(\sum_i \mathbf{x}_i^{(N)}) \\ \mathbf{f}_i &:= \kappa_{\theta}(\mathbf{x}_i^{(N)}) \end{aligned} \quad (17)$$

As explained above, the nuclear and electronic cusp conditions are built into the architecture via φ_{μ} and γ , and the Jastrow factor and backflow must be cusplless for them not to break the cusp behavior (see eq. 15). This translates into the requirement that the distance featurization $\mathbf{e}(r)$ is cusplless, since that is the only point via which the interparticle distances enter the SchNet architecture. We use a featurization inspired by the PhysNet architecture (Unke and Muwly, 2019), with a modified envelope that forces all the Gaussian features and their derivatives to zero at zero distance (Figure 2),

$$\begin{aligned} e_k(r) &:= r^2 e^{-r - (r - \mu_k)^2 / \sigma_k^2}, \\ \mu_k &:= r_c q_k^2, \quad \sigma_k := (1 + r_c q_k) / 7 \end{aligned} \quad (18)$$

where q_k equidistantly spans the interval (0, 1) and r_c is a cutoff parameter.

2.3 Sampling electronic wave functions

To generate samples of \mathbf{r} from the wave-function distribution $|\psi^2(\mathbf{r})|$, needed to evaluate the expected value in (6), we use a standard Langevin Monte Carlo approach commonly used in VMC (Umrigar et al., 1993). Langevin Monte Carlo is based on the standard Metropolis–Hastings algorithm, with a modified proposal step to achieve more efficient sampling of electronic wave functions. The proposal step is defined by a time discretization of the overdamped Langevin equation, where a Gaussian random vector $\boldsymbol{\eta}$ and a step along the current *quantum force* are added to the electronic coordinates,

$$\mathbf{r} := \mathbf{r} + \nabla \ln |\psi(\mathbf{r})| \tau + \boldsymbol{\eta} \sqrt{\tau} \quad (19)$$

Umrigar et al. (1993) devised several techniques to avoid numerical problems due to large changes in the quantum force when electrons are close to the nodes or nuclei, which we use with one extra simplification. Rather than proposing electronic steps in spherical coordinates close around the nuclei, we clip the step length such that the step size is always shorter than the distance to the nearest nucleus, so the nucleus can never be “overshot”.

The initial electron positions for the Markov chain are sampled from Gaussian distributions around the nuclei such that the effective atomic Mulliken charges obtained from the HF method are respected.

2.4 Training the network

To optimize the parameters θ in the Jastrow and backflow neural networks and minimize the electronic energy, we use the standard Adam optimizer (Kingma and Ba, 2014) together with the variational energy from (6) used directly as the loss function. To calculate the stochastic gradient of the loss function over a batch of samples, we use a gradient formula that takes advantage of the fact that the Hamiltonian operator in (5) is Hermitian (Ceperley et al., 1977),

$$\begin{aligned}\mathcal{L}(\theta) &= \mathbb{E}_{\mathbf{r} \sim |\psi|^2} [E_{\text{loc}}(\mathbf{r}; \theta)] \\ \nabla_{\theta} \mathcal{L}(\theta) &= 2 \mathbb{E}_{\mathbf{r} \sim |\psi|^2} [(E_{\text{loc}}(\mathbf{r}; \theta) - \mathcal{L}(\theta)) \nabla_{\theta} \ln |\psi_{\theta}|]\end{aligned}\quad (20)$$

This expression for the gradient requires calculating only second derivatives of the wave function (for the Laplace operator), whereas direct differentiation would require third derivatives (derivative of the Laplace operator), which is computationally costly and numerically unstable. Note that although wave functions in VMC are usually optimized on a fixed sample of electron positions using deterministic optimization methods, stochastic gradient descent has been previously tested for traditional wave function forms in VMC with good results (Harju et al., 1997).

Similarly to the quantum force used in sampling of the wave function, the parameter gradients can grow very large when the electrons approach the nodal surface or the nuclei, which makes the optimization unstable. We circumvent this issue by clipping the parameter gradients by the same amount by which the algorithm of Umrigar et al. (1993) clips the quantum force.

We use each sampled electron configuration \mathbf{r} only once in an optimization run.

2.5 Computational details

All the reported methods were implemented in Pytorch and run on a single GTX 1080 Ti GPU. The linear coefficients of the HF orbitals φ_{μ} were calculated with PySCF (Sun et al., 2018) using the “6-311G” Gaussian basis set. The plain fully-connected DNNs that represent the trainable functions in our architecture were chosen such the total number of trainable parameters is around 7×10^4 . We have found that a relatively large batch size of several thousand electronic samples leads to the most efficient training.

3 Results

In this work, we test only the Jastrow part of our architecture and turn the backflow part off, which means that the nodal surface

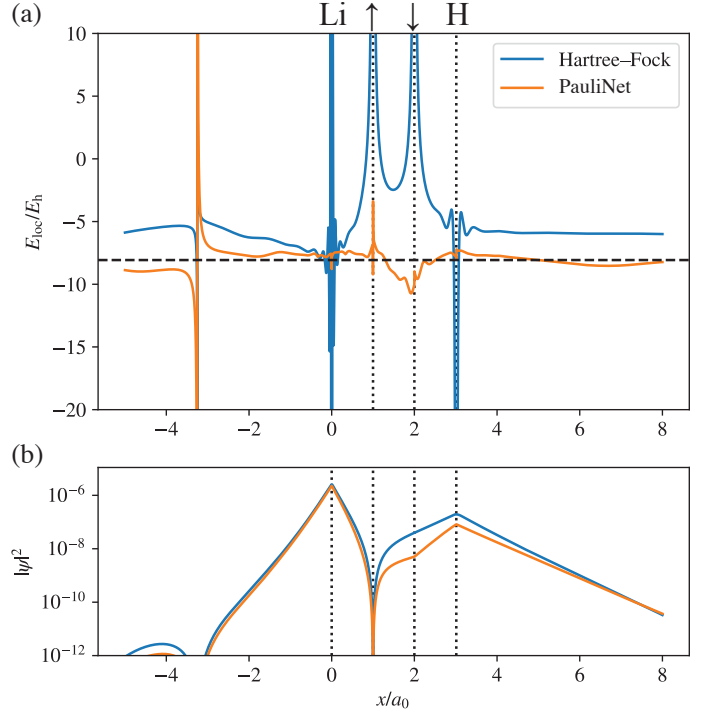


Figure 3 | One-dimensional scan of the wave function and its local energy in LiH. The Li and H nuclei, two spin-up and one spin-down electrons are put on the x -axis, the fourth electron is positioned randomly off the axis, and the x -coordinate of the first electron is varied. The divergence of the local energy at around $x = -3$ is caused by a nodal surface.

of the optimized wave function is inherited from the HF method. This enables us to directly compare against fixed-node DMC calculations. We use the same set of atoms and small molecules that were used to test DeepWF (Han et al., 2018), in particular H_2 , LiH, Be, B, and the linear hydrogen chain H_{10} (Table 1).

3.1 PauliNet outperforms state-of-the-art Jastrow factors

First, we investigate atoms and diatomic molecules, in which the single-determinant description of the HF method is appropriate, and the Jastrow factor needs to capture only the so-called dynamic correlation of the electrons. A common way to compare the accuracy of *ab-initio* methods in quantum chemistry is via the fraction of *correlation energy* captured, defined as the difference between the exact ground-state energy and that of the HF method.

Whereas DeepWF does not even reach the accuracy of the HF method for LiH and B, our PauliNet gives variational energies that are better than those from state-of-the-art VMC calculations, and are only outperformed by the fixed-node limits of DMC calculations by several percents of the correlation energy. Besides any potential inherent limitations of our Jastrow factor, the difference to fixed-node DMC is partially due to the backflow part being switched off, and the quality of the nodal surface is thus limited by the small basis set used for $\varphi_{\mu}(\mathbf{r})$. Calculations were extremely fast compared to the timing benchmarks reported by Pfau et al. (2019). It took several hundreds of iterations to converge the energy to the reported values, corresponding to tens of minutes on a single GTX 1080 Ti GPU.

The total electronic energy is a global measure of the quality of the wave function, but does not necessarily portray whether

Table 1 | Ground-state energies of five test systems obtained by four different methods.

| system ^a | VMC | | DMC | E_0/E_h (% E_{corr}) | | DeepWF | PauliNet | |
|------------------------------|-----------------------|-------|-----------------------|----------------------------------|----------|--------------|-------------|--------------|
| H ₂ ^b | | | | | | -1.1738 | 98.4% | -1.174 37(6) |
| LiH ^c | -8.0635 ^f | 91.5% | -8.0703 ^f | 99.7% | -7.8732 | ^g | -8.0690(3) | 98.1% |
| Be ^d | -14.6311 ^d | 61.6% | -14.6572 ^d | 89.2% | -14.6141 | 43.6% | -14.6546(7) | 86.5% |
| B ^d | -24.6056 ^d | 60.0% | -24.6398 ^d | 88.3% | -24.2124 | ^g | -24.634(2) | 83.5% |
| H ₁₀ ^e | | | | | -5.5685 | 63.8% | -5.655(2) | 96.0% |

^aFootnotes contain references to references exact ground-state energies, and HF energies for calculation of the correlation energy. ^bKołos and Wolniewicz (1965). ^cCencek and Rychlewski (2000). ^dBrown et al. (2007). ^eMotta et al. (2017). ^fCasalegno et al. (2003). ^gFor LiH and B, DeepWF does not reach the accuracy of the HF method.

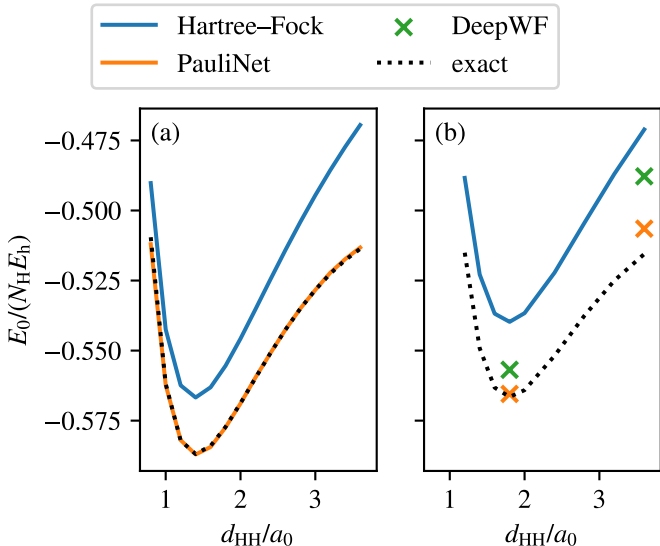


Figure 4 | Electronic energy as a function of distance between hydrogen atoms in H₂ (a) and H₁₀ (b). The exact values are calculated with FCI@cc-pvQZ for H₂ and taken from Motta et al. (2017) for H₁₀.

the wave function is reasonable even in low-probability regions. Especially with the use of DNNs one could doubt whether the wave function behaves correctly in regions that might not have been even represented in the training data. Figure 3 shows that PauliNet generalizes well to such regions. Even though the chosen electron configuration has a very low probability ($|\psi|^2$ orders of magnitude lower than for the most likely configurations), the DNN learned to modify the HF wave function in such a way that the local energy shifts towards the exact value along the whole scan. The plot also illustrates the correct representation of the nuclear and electronic cusps, as the local energy of the PauliNet wave function does not diverge nor oscillate around the coalescence points.

3.2 PauliNet captures strong correlation

Unlike the atoms and diatomics, the linear hydrogen chain H₁₀ exhibits *strong correlation*, which describes a situation where the (restricted) single-determinant description of the HF method is insufficient, and the correlation energy constitutes a significant part

of the electronic energy (Motta et al., 2017). In essence, the HF wave function in strongly-correlated systems allows many electronic configurations which have a large local energy. A relatively straightforward remedy from quantum chemistry is to use a linear combination of multiple determinants, each of them allowing different subsets of electronic configuration in a coordinated fashion. An alternative approach, applicable in VMC, is to have a Jastrow factor with very small values for all electronic configurations that have large local energies. This is a hard test for a Jastrow factor, because distinguishing the high-energy electronic configurations is a complicated function of the positions of all the electrons with respect to each other and to the nuclei, not just of the electron distances (Goetz and Neuscamman, 2017).

Already H₂ exhibits strong correlation when the two atoms are dissociated, but our Jastrow factor is able to cover the transition from dynamic to strong correlation smoothly, recovering more than 99% of the correlation energy along the whole dissociation curve (Figure 4a).

For H₁₀, we recover 96% (80%) of the exact correlation energy in the equilibrium (stretched) geometry (Figure 4b). The decrease of the captured fraction of the correlation energy with larger atom separations illustrates the increased difficulty of the problem due to the strong correlation. The supposedly harder problem of learning the Jastrow factor for a strongly-correlated system leads to a longer optimization time, here on the order of hours for H₁₀.

4 Discussion

We have shown that DNN representations of electronic wave functions in real space have the potential to outperform state-of-the-art variational ansatzes. Compared to standard functional forms used in VMC, the use of DNNs has several advantages. The much higher flexibility of DNNs allows VMC to reach the accuracy of DMC, in principle enabling easier calculation of accurate derived electronic properties beyond the electronic energy. Besides encoding more complex many-body correlations between electrons, the DNNs have an essentially unlimited flexibility in the spatial degrees of freedom, circumventing the plague of incomplete basis sets of quantum chemistry, which can be removed only with DMC when using standard techniques. Furthermore, the wild oscillations of the local energy close to heavy nuclei require the use of pseudopotentials for heavier elements such as transition metals in standard QMC calculations. The flexibility

of DNNs could sidestep this necessity by smoothing out these oscillations, which cannot be done with standard wave-function ansatzes. Strong correlation is usually treated by using multi-determinant expansions, which are computationally demanding and introduce the problem of selecting the proper subset of determinants. Treating strong correlation on the level of Jastrow factors traditionally requires construction of specialized many-body forms (Goetz and Neuscamman, 2017). In contrast, DNNs are capable of learning strong correlation between electrons without any specific adaptation. Finally, experience from molecular force fields shows that DNNs are able to learn universal force fields that can generalize across the chemical space. This hints at the possibility of training universal wave functions with a single functional form valid over a range of molecular geometries.

In parallel, Pfau et al. (2019) developed a deep-learning architecture similar to ours, and already a brief comparison between the two hints at potential improvements of both. In particular, the combination of built-in physical constraints as done in PauliNet and approximate second-order optimization techniques used for PauliNet has the potential to keep the very high accuracy of the latter while reaching the relatively low computational cost of the former. Detailed benchmarks of the different aspects of the two approaches, and search for the optimal combination, as well as further improvement of the DNN architecture are a straightforward topic for future work. We hope that the introduction of DNNs into the field of quantum Monte Carlo opens the possibility to utilize the striking advances in deep learning from the last decade in a new field.

Acknowledgments

Funding is acknowledged from the European Commission (ERC CoG 772230 “Scale-Cell”), Deutsche Forschungsgemeinschaft (CRC1114/A04, GRK2433 DAEDALUS/P04), the MATH⁺ Berlin Mathematics research center (AA1x6, EF1x2). J. H. would like to thank K.-R. Müller for support and acknowledge funding from TU Berlin (Project No. 10032745).

References

- B. M. Austin, D. Y. Zubarev, and W. A. Lester. Quantum Monte Carlo and Related Approaches. *Chem. Rev.*, 112(1):263–288, Jan. 2012. doi:10.1021/cr2001564.
- M. D. Brown, J. R. Trail, P. López Ríos, and R. J. Needs. Energies of the first row atoms from quantum Monte Carlo. *J. Chem. Phys.*, 126(22):224110, June 2007. doi:10.1063/1.2743972.
- G. Carleo and M. Troyer. Solving the Quantum Many-Body Problem with Artificial Neural Networks. *Science*, 355(6325):602–606, Feb. 2017. doi:10.1126/science.aag2302.
- M. Casalegno, M. Mella, and A. M. Rappe. Computing accurate forces in quantum Monte Carlo using Pulay’s corrections and energy minimization. *J. Chem. Phys.*, 118(16):7193, 2003. doi:10.1063/1.1562605.
- W. Cencek and J. Rychlewski. Benchmark calculations for Heq2 and LiH molecules using explicitly correlated Gaussian functions. *Chem. Phys. Lett.*, 320:549–552, 2000.
- D. Ceperley, G. V. Chester, and M. H. Kalos. Monte Carlo simulation of a many-fermion study. *Phys. Rev. B*, 16(7):3081–3099, Oct. 1977. doi:10.1103/PhysRevB.16.3081.
- D. M. Ceperley. Fermion nodes. *J. Stat. Phys.*, 63(5-6):1237–1267, June 1991. doi:10.1007/BF01030009.
- N. D. Drummond, M. D. Towler, and R. J. Needs. Jastrow correlation factor for atoms, molecules, and solids. *Phys. Rev. B*, 70(23):235119, Dec. 2004. doi:10.1103/PhysRevB.70.235119.
- W. M. C. Foulkes, L. Mitas, R. J. Needs, and G. Rajagopal. Quantum Monte Carlo simulations of solids. *Rev. Mod. Phys.*, 73(1):33–83, Jan. 2001. doi:10.1103/RevModPhys.73.33.
- B. V. D. Goetz and E. Neuscamman. Suppressing Ionic Terms with Number-Counting Jastrow Factors in Real Space. *J. Chem. Theory Comput.*, 13(5):2035–2042, May 2017. doi:10.1021/acs.jctc.7b00158.
- J. Han, L. Zhang, and W. E. Solving Many-Electron Schrödinger Equation Using Deep Neural Networks. *arXiv*, 1807.07014, July 2018. URL <http://arxiv.org/abs/1807.07014>.
- A. Harju, B. Barbiellini, S. Siljamäki, R. M. Nieminen, and G. Ortiz. Stochastic Gradient Approximation: An Efficient Method to Optimize Many-Body Wave Functions. *Phys. Rev. Lett.*, 79(7):1173–1177, Aug. 1997. doi:10.1103/PhysRevLett.79.1173.
- T. Kato. On the eigenfunctions of many-particle systems in quantum mechanics. *Commun. Pure Appl. Math.*, 10(2):151–177, Jan. 1957. doi:10.1002/cpa.3160100201.
- D. P. Kingma and J. Ba. Adam: A Method for Stochastic Optimization. *arXiv*, 1412.6980, Dec. 2014. URL <http://arxiv.org/abs/1412.6980>.
- W. Kolos and L. Wolniewicz. Potential-Energy Curves for the $X\ 1\Sigma^+_g$, $b^3\Sigma^+_u$, and $C\ 1\Pi_u$ States of the Hydrogen Molecule. *J. Chem. Phys.*, 43(7):2429–2441, Oct. 1965. doi:10.1063/1.1697142.
- P. López Ríos, A. Ma, N. D. Drummond, M. D. Towler, and R. J. Needs. Inhomogeneous backflow transformations in quantum Monte Carlo calculations. *Phys. Rev. E*, 74(6), Dec. 2006. doi:10.1103/PhysRevE.74.066701.
- D. Luo and B. K. Clark. Backflow Transformations via Neural Networks for Quantum Many-Body Wave Functions. *Phys. Rev. Lett.*, 122(22):226401, June 2019. doi:10.1103/PhysRevLett.122.226401.
- A. Ma, M. D. Towler, N. D. Drummond, and R. J. Needs. Scheme for adding electron–nucleus cusps to Gaussian orbitals. *J. Chem. Phys.*, 122(22):224322, June 2005. doi:10.1063/1.1940588.
- M. Motta, D. M. Ceperley, G. K.-L. Chan, J. A. Gomez, E. Gull, S. Guo, C. A. Jiménez-Hoyos, T. N. Lan, J. Li, F. Ma, A. J. Millis, N. V. Prokof’ev, U. Ray, G. E. Scuseria, S. Sorella, E. M. Stoudenmire, Q. Sun, I. S. Tupitsyn, S. R. White, D. Zgid, S. Zhang, and Simons Collaboration on the Many-Electron Problem. Towards the Solution of the Many-Electron Problem in Real Materials: Equation of State of the Hydrogen Chain with State-of-the-Art Many-Body Methods. *Phys. Rev. X*, 7(3):031059, Sept. 2017. doi:10.1103/PhysRevX.7.031059.
- R. J. Needs, M. D. Towler, N. D. Drummond, and P. L. Ríos. Continuum variational and diffusion quantum Monte Carlo calculations. *J. Phys. Condens. Matter*, 22(2):023201, Jan. 2010. doi:10.1088/0953-8984/22/2/023201.
- D. Pfau, J. S. Spencer, A. G. d. G. Matthews, and W. M. C. Foulkes. Ab-Initio Solution of the Many-Electron Schrödinger Equation with Deep Neural Networks. *arXiv*, 1909.02487, Sept. 2019. URL <http://arxiv.org/abs/1909.02487>.
- L. Piela. *Ideas of Quantum Chemistry*. Elsevier, 2nd edition, 2014. ISBN 978-0-444-52227-6.
- K. T. Schütt, H. E. Sauceda, P.-J. Kindermans, A. Tkatchenko, and K.-R. Müller. SchNet – A deep learning architecture for molecules and materials. *J. Chem. Phys.*, 148(24):241722, June 2018. doi:10.1063/1.5019779.
- K. T. Schütt, M. Gastegger, A. Tkatchenko, K.-R. Müller, and R. J. Maurer. Unifying machine learning and quantum chemistry – a deep neural network for molecular wavefunctions. *arXiv*, 1906.10033, June 2019. URL <http://arxiv.org/abs/1906.10033>.
- Q. Sun, T. C. Berkelbach, N. S. Blunt, G. H. Booth, S. Guo, Z. Li, J. Liu, J. D. McClain, E. R. Sayfutyarova, S. Sharma, S. Wouters, and G. K.-L. Chan. PySCF: The Python-based simulations of chemistry framework. *WIREs Comput. Mol. Sci.*, 8(1):e1340, Jan. 2018. doi:10.1002/wcms.1340.
- A. Szabo and N. S. Ostlund. *Modern Quantum Chemistry: Introduction to Advanced Electronic Structure Theory*. Revised edition, 1996. ISBN 0-486-69186-1.
- M. Troyer and U.-J. Wiese. Computational Complexity and Fundamental Limitations to Fermionic Quantum Monte Carlo Simulations. *Phys. Rev. Lett.*, 94(17):170201, May 2005. doi:10.1103/PhysRevLett.94.170201.
- C. J. Umrigar, M. P. Nightingale, and K. J. Runge. A diffusion Monte Carlo algorithm with very small time-step errors. *J. Chem. Phys.*, 99(4):2865–2890, Aug. 1993. doi:10.1063/1.465195.
- O. T. Unke and M. Meuwly. PhysNet: A Neural Network for Predicting Energies, Forces, Dipole Moments and Partial Charges. *arXiv*, 1902.08408, Feb. 2019. URL <http://arxiv.org/abs/1902.08408>.
- T. Van Voorhis and M. Head-Gordon. Benchmark variational coupled cluster doubles results. *J. Chem. Phys.*, 113(20):8873–8879, Nov. 2000. doi:10.1063/1.1319643.